Modelling the vibrational behaviour of composite archery arrows

Marianne Rieckmann (1), John Codrington (1) and Ben Cazzolato (1)

(1) School of Mechanical Engineering, University of Adelaide, SA, Australia

ABSTRACT

In the sport of archery, recent developments in materials technology have seen the introduction of carbon-fibre aluminium composite arrows. Archery performance has been shown to be dependent on the vibrational behaviour of arrows (including the natural frequencies and mode shapes). This paper investigates the vibration of composite archery arrows through analytical and finite element modelling. Computer models used in this paper employ modal analysis to identify the significant modes of vibration. Results from the numerical simulations are also compared to experimental measurements using a Polytec scanning laser Doppler vibrometer (PSV-400). Experiments use both mechanically and acoustically coupled vibration actuators to vibrate the composite arrow structure. Evaluation of the modal behaviour shows good agreement between the theoretical models and the experiments.

INTRODUCTION

Using composite materials in the design of archery arrows offers the advantage of high strength and stiffness combined with low weight. The composite arrow material comprises of unidirectional carbon fibre and epoxy resin matrix fused to a high tensile aluminium alloy core tube. Composite arrows have been designed to minimise the aerodynamic drag by a using a smaller diameter shaft when compared to arrows made entirely of aluminium alloy. The use of composite materials has allowed this optimisation while still retaining the required stiffness for archery performance. However, the low transverse strength of the orthotropic composite material has the disadvantage of delamination or subsurface cracks when exposed to fatigue and impact loads.

Archery performance depends on the proper matching of arrow to bow. The flexural rigidity of the arrow, also called the arrow spine, should allow one full cycle of oscillation by the time it leaves the bow (Klopsteg, 1943). For best performance the arrow must bend around the bow and avoid any contact that may deflect the arrow from its desired trajectory. One problem that archers face is the identification of damaged arrows that have lost structural integrity, and will exhibit changed dynamic performance when shot from a bow.

After the arrow leaves the bow, the free-flight of the arrow has been shown to have bending modes of vibration (Zanevskyy, 2001). This affects the aerodynamic performance since the lowest aerodynamic drag will be achieved when the arrow's path is approximately straight with a zero angle of attack.

The motivation for this paper is to perform a preliminary investigation into the composite archery arrows to gain a base line for comparison to damaged arrows in future studies. Vibration prediction and modelling is important for monitoring the structural health of composite materials and understanding their performance in-service.

VIBRATION OF ARCHERY ARROWS

Composite archery arrow shafts are long thin cylindrical shells with a multi-layer wall of variable thickness. A complete assembled arrow will have a nock on one end, a point weight on the other, and vanes or fletches as shown in Figure 1. The vibration analysis of archery arrows should take into account this physical composite structure. In this paper the focus will be on evaluation of the modal behaviour of archery arrow shafts without considering the point masses of the nock, point and fletches.
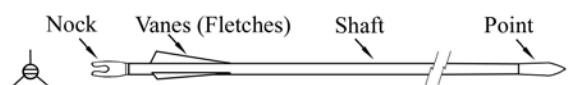
Figure 1. Complete assembled arrow

The vibration behaviour of archery arrows is highly complex. The long slender geometry leads to beam-like behaviour, while the hollow tubular cross-section also gives rise to shell modes of vibration. The large thickness to radius ratio means that thin-shell theory does not perfectly capture the dynamics and the varying thickness along the length further complicates the modal response. The different behaviours may be analysed using known theories of beam and shell vibrations to determine natural frequencies and mode shapes. Relevant literature for the range of vibrational behaviours is reviewed in this section to determine the most appropriate approaches for modelling a composite archery arrow.

Vibration of a beam in bending considers the displacements perpendicular to its length. These vibrations are often called transverse or flexural vibrations. Transverse vibration analysis of a beam usually employs simple beam theory, which assumes that the beam has uniform cross-section. It is also assumed that the plane of symmetry of the beam is the plane of vibration. The vibration of a bar can be considered when displacements are axially aligned along the length of the object. The beam and bar approximations are considered suitable for long shells with the length to radius ratio > 20

(Forsberg, 1966). The different modes of vibration are dependent on the boundary constraints. In this study, the primary interest is of free-free boundary conditions for a cylindrical beam.

While beam theory may be most suited to the long slender structure of the arrow, shell theories are required to capture the cross-sectional modes. There are many shell theories that can be applied to cylindrical shells, including both thin and thick-walled shells. These theories are derived from strain-displacement equations, force and moment resultants, and equations of motion (Leissa, 1993). Differing assumptions for which terms can be neglected in the derivation produce approximate solution shell theories with varying complexity. For example, rotary inertia and shear deformation is generally neglected unless the shells become relatively thick, with the thickness to radius ratio < 1/10 (Leissa, 1993). The main factor to consider is if membrane forces dominate or bending effects dominate the vibrational behaviour. Physical parameters such as the thickness to radius ratio, the length to radius ratio, and the boundary conditions will determine the most appropriate analytical theory for a given application.

Typical vibration modes of cylindrical shells are shown in Figure 2. The circumferential modal indices $n=0,1,2,3\ldots$ indicate the number of waves around the circumference of the cylinder. The axial modal indices $m=0,1,2,3\ldots$ indicate the waves along the length of the cylinder. The number of axial nodes will depend on the end boundary conditions. For the free-free boundary conditions and axial modal index of $m=1$, there will be one axial node line of minimum vibration. The axial nodal patterns shown in Figure 2 are the out-of-plane motion for opposite sides of the cylinder. This motion will be in phase when the circumferential mode index n is even and out of phase when the circumferential mode index n is odd. In a cylinder, displacements in the circumferential, axial and radial directions must be considered to accurately capture the dynamic behaviour (Fahy and Gardonio, 2007). Independent modes occur in the circumferential, axial and radial directions.

Circumferential nodal patterns

Axial nodal patterns for free-free boundary conditions

Circumferential node

Axial node
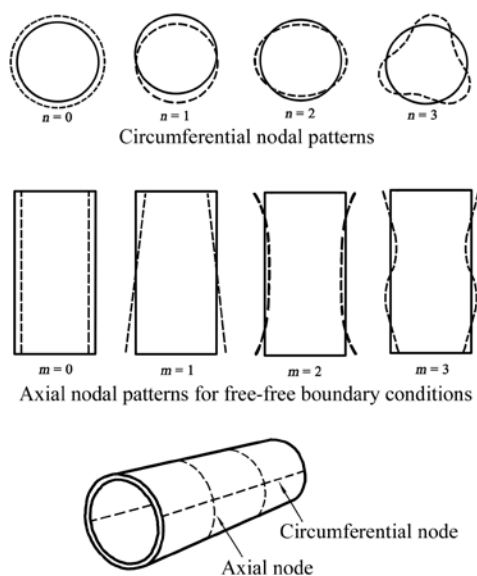
Figure 2. Cylindrical shells modes of vibration, adapted from (Forsberg, 1966) and (Egle and Sewall, 1968).

The multi-layered composite cylinder of archery arrows may be considered as thick-walled and as such, thin-shell theory for cylindrical structures may not always be valid (Hamidza-

deh and Jazar, 2010). Analytical solutions become increasingly complex as the wall thickness increases and when the different layer properties (often orthotropic) are included. Furthermore, archery arrows can have variable thickness carbon fibre layer, which is tapered for aerodynamic performance. The derivation of a closed-form solution for shells having continuously variable wall thickness is essentially intractable (Leissa, 1993). Cylinders of variable thickness are sometimes modelled in the form of a step discontinuity in the thickness at some point along the length of the cylinder in order to reduce the complexity (Leissa, 1993).

The review of relevant literature presented here covers a small portion of the large range of studies into cylindrical shells. The constraints that limit the analytical solution will be the physical parameters of the structure, which determine when membrane effects dominate or when the bending effects will dominate the vibrational behaviour. The relevance of each shell theory to a particular cylindrical structure will depend on the length to radius ratio and the thickness to radius ratio. For a composite archery arrow that is a long and thin cylindrical shape with relatively thick walls, it is clear that the bending effects will dominate and beam theory is most appropriate to calculate the dominant natural frequencies.

Archery arrow specimens

The arrow specimens used in the experiments included an all aluminium arrow, as well as two different composite arrows. The aluminium arrow is a Superlite1713 shaft and the composite arrows are Protour570 and Protour380 shafts that where donated by Easton Technical Products (see Figure 3).

Figure 3. Archery arrow specimens, pictured from left to right the ProTour570, Superlite1713 and ProTour380.

The physical dimensions of the arrow specimens where taken from the manufacturers specifications (Easton, 2011) as well as measurements. The outer diameter of the tested arrows was measured using a micrometer and the average radius profiles are shown in Figure 4. These dimensions where used to create the FE models of the composite arrows. Two specimens of the aluminium arrow, and three specimens of each composite arrow were tested to provide a good statistical average for each vibrational experiment. The arrow specimens used in the experiment include whole stock length shafts without the nock and point installed. It is expected that future work will be performed on fully assembled arrows with nocks and points.
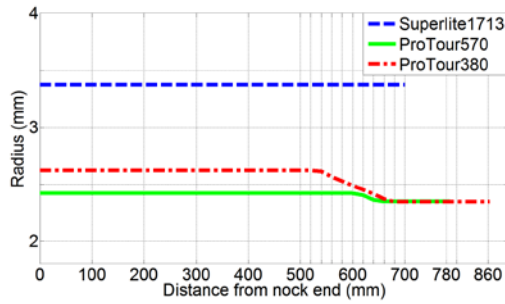
Figure 4. Profiles of archery arrow specimens

The size of the composite arrow shaft is defined as the static spine of the arrow, that is the deflection of the arrow in thousandths of an inch, when a 880gram (1.94 lbs.) is suspended from the centre of the arrow that is supported at two points 711mm (28 inches) apart (Park, 2011). For example, the Pro-Tour570 will have a deflection of 14.578mm (570/1000 inch) when tested for static spine (Easton, 2011). The static spine test is useful for estimating unknown material properties of the composite arrow such as the Young's modulus.

ANALYTICAL CALCULATIONS

Typical analytical approaches to estimate the natural frequencies of the arrow specimens use beam theory for the low frequency modes of vibration, and thin shell theory for high frequency modes.

Beam and Bar theory

In the case of a beam type vibration of a circular cylindrical shell, it can be justified theoretically that basic equations of vibration of a thin shell cylinder can be reduced to the transverse vibrations of a beam provided that the length to radius ratio is much greater than unity (Kornecki, 1971). The slender beam theory, often refereed to as Euler-Bernoulli beam equation, is based on the assumption that shear deformation is much smaller than the transverse or bending deformation. For boundary conditions of a free-free beam the weighted frequencies $\beta_a l$ are listed in Table 1. To keep consistent subscripts, the bending mode number a is used, where $a=1$ is the first bending mode of the beam with frequency of ω_a. This first bending mode is equivalent to the cylindrical mode of vibration with circumferential mode of $n=1$, and axial mode of $m=2$. The formula for the natural frequency ω is given in Table 1.

Table 1. Weighted natural frequencies for free-free boundary conditions (Inman, 2001)

a	$\beta_a l$
0	0 (rigid-body mode)
1	4.73004074
2	7.85320462
3	10.9956078
4	14.1371655
5	17.2787597
> 5	$(2a + 1)\,\pi/2$

$$\omega_{(n=1,\ m=a+1)} = \omega_a = (\beta_a l)^2 \ \sqrt{E\,I / (\rho\,A\,l^4)}$$

where a is the bending mode number,
E is Young's modulus, I is the moment of inertia,
ρ is the density, A is the cross section area,
and l is the length of the beam.

For the bar type vibrations of a cylinder the natural frequency ω_b where b is the bar (or extension) mode number, may be found using (Inman, 2001).

$$\omega_b = (b\,\pi\,\sqrt{(E / \rho)})\,/\,L \tag{1}$$

where b is the bar (or extension) mode number, E is Young's modulus, ρ is the density of the shell material, and L is the length of the cylinder.

Thin shell theory

Free-free boundary conditions will be used for the arrow shafts. For this configuration some examples of vibrational modes are shown in Figure 5. In this current work, the two theories used to find the circumferential modes of vibration of the cylinder were the Love-Timoshenko theory for cylindrical shells of infinite length (Leissa, 1993), and Rayleigh's inextensional theory of shells (Leissa, 1993). These theories result in the non-dimensional frequency parameter Ω given in Equation (2).

Bending mode for $n=1$, $m=2$

Radial breathing mode for $n=0$, $m=1$

Extension mode for $n=0$, $m=0$

Torsional mode for $n=0$
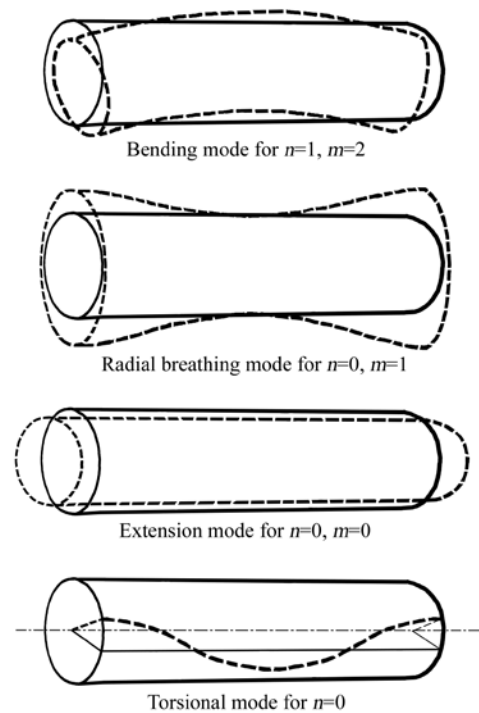
Figure 5. Examples of vibrational modes of a cylinder, adapted from (Hamidzadeh and Jazar, 2010).

$$\Omega^2 = (\rho\,(1 - \nu^2)\,R^2\,\omega^2)\,/\,E \tag{2}$$

where ρ is the density of the shell material, ν is Poisson's ratio, R is the radius of the cylinder, ω is the natural frequency, and E is Young's modulus.

The radial and circumferential modes of vibration in the Love-Timoshenko theory are calculated using Equation (3). The lowest values found from this formula will be the circumferential modes of vibration for $n >= 2$.

$$\Omega^2 = \tfrac{1}{2}(\,(1 + n^2)(1 + kn^2)$$
$$\pm \sqrt{((1 + n^2)^2 - 2kn^2(1 - 6n^2 + n^4))}\,) \tag{3}$$

where n is the circumferential mode index and k is the non-dimensional thickness parameter given in Equation (5).

Natural frequencies and mode shapes for a cylinder with free-free boundary conditions may be obtained using the inextensional theory formulated by Rayleigh (Leissa, 1993). The inextensional theory of shells, that requires middle surface

deformation without stretching, is calculated using Equation (4) and correlates well with the Love-Timoshenko circumferential modes of vibration.

$$\Omega^2 = k\, n^2 (n^2-1)^2 / (1+n^2) \qquad (4)$$

In the previous equation k is the nondimensional thickness parameter given in Equation (5) and n is the circumferential mode index.

$$k = h^2 / 12R^2 \qquad (5)$$

where h is the thickness of the shell and R is the radius.

The thin shell theories were used to calculate the circumferential modes when $n=2$ and $n=3$. These approximate thin shell theories have good agreement and will converge to the exact theory for the higher circumferential modes, but are not suitable for calculating modes where $n < 2$ (Leissa, 1993).

FINITE ELEMENT MODELLING

Finite element (FE) analysis was conducted to investigate all of the modes of vibration (beam and shell) of the composite archery arrow. The FE models were developed in ANSYS Workbench 12.1 using multi-layered quadratic shell elements (SHELL281). A single shell element represented the full thickness of the arrow wall with 12 elements around the circumference (see Figure 6). The shell body was mapped meshed (typical element aspect ratio 1:1) to give around 600 element divisions along the arrow length, which ranged from 700-900mm. A total of 5000-9500 elements were used, depending on the length of the model. Three FE models were developed, the first for an all aluminium arrow, and another two for the composite arrows. The aim of the aluminium isotropic model is for validation of the FE procedure against isotropic analytical models. The composite FE models build on the isotropic model by adding a layer of orthotropic material for the carbon epoxy material. Eigenvalue modal analyses were conducted using ANSYS to obtain the natural frequencies and mode shapes.
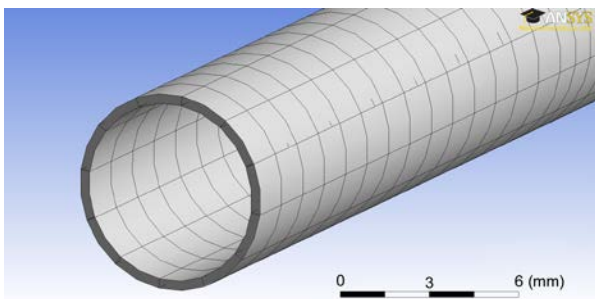
Figure 6. Meshed Arrow

Aluminium cylindrical shell model

A FE model of an aluminium cylindrical shell was created to match the physical properties of an aluminium arrow shaft with length of 700mm, nominal diameter of 6.747mm (17/64 inch), and wall thickness of 0.33mm (13/1000 inch). These dimensions correspond to a Superlight1713 arrow, which is made of AL7075-T9 aluminium and has a density of ρ=2800kg/m³, Poisson ratio of ν=0.33, and Young's modulus of E=72GPa (Gere, 2001). The shell surface body of the arrow was mapped with face meshing to give a total of 5208 elements.

The natural frequencies for the cylindrical and bending modes were obtained and are compared against the analytical calculations from the beam and bar theory using Table 1 and Equation (1), and the thin shell theory using Equations (2) through (5). The results for the natural frequencies are given in Table 2 along with the mode indices.

Table 2. Comparison of natural frequencies for an aluminium cylindrical arrow using analytical expressions and FEA

Analytical f_A (Hz)	FEA f_{FE} (Hz)	%err $\Delta f/f_A$	Mode indices
	0		Translation modes
84[a]	84	0	$n=1$, $m=2$ bending
231[a]	230	0	$n=1$, $m=3$
453[a]	451	0	$n=1$, $m=4$
748[a]	743	-1	$n=1$, $m=5$
1118[a]	1107	-1	$n=1$, $m=6$
1561[a]	1541	-1	$n=1$, $m=7$
2078[a]	2044	-2	$n=1$, $m=8$
	2222		$n=0$, $m=1$ breathing
2669[a]	2613	-2	$n=1$, $m=9$
3334[a]	3248	-3	$n=1$, $m=10$
3622[b]	3622	0	$n=0$, $m=0$ extension
4073[a]	3947	-3	$n=1$, $m=11$
	4443		$n=0$, $m=2$ breathing
4886[a]	4706	-4	$n=1$, $m=12$
21210[c]	21260		$n=2$, $m=1$
59990[c]	62310		$n=3$, $m=1$

where $\Delta f = f_{FE} - f_A$

Vibrational modes above 5kHz have been omitted, except for higher order circumferential modes for n=2 and n=3.
[a] Beam theory calculated from Table 1.
[b] Bar theory calculated from Equation (1).
[c] Shell theories calculated from Equations (2) through (5).

As seen in the analytical and FE model simulations, bending dominates the first modes of vibration. The circumferential modes of $n=2$ and $n=3$ predicted by the thin-shell theories occur above 20kHz. The beam theory and FE results have good agreement for the first six natural frequencies, and are within 4% for all frequencies below 5kHz. This divergence is consistent with the beam theory where the assumptions will not be appropriate when the wavelength of a bending mode is less than 20 times the radius (Forsberg, 1966). In this case, for the Superlite1713 arrow, this occurs for axial mode indices of $m>20$. The results show that the simple model of an isotropic cylinder validates the FE process and provides confidence in building upon the isotropic models for the composite cylinder models. The first and second bending mode shapes, and the first breathing mode shape are shown in Figures 7, 8, and 9 respectively.
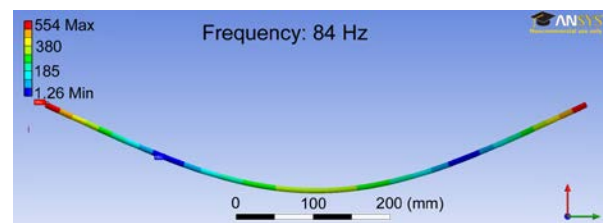
Figure 7. FE first bending mode of aluminium cylinder, modal indices $n=1$, $m=2$
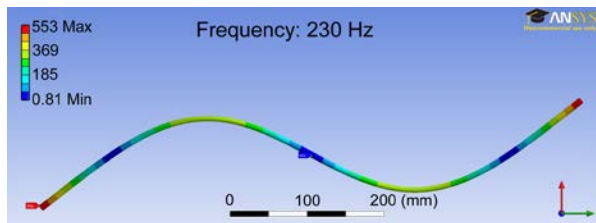
Figure 8. FE second bending mode of aluminium cylinder, modal indices n=1, m=3
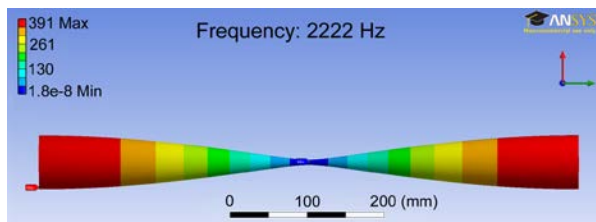
Figure 9. FE first breathing mode of aluminium cylinder, modal indices n=0, m=1

Composite archery arrow models

A FE model of the two composite arrows was defined to match the physical properties of ProTour570 and ProTour380 arrows. These arrows have a core of AL7075-T9 aluminium with an outer diameter of 3.572mm (9/64 inch) and a thickness of 0.1524mm (6/1000 inch) with the same material properties as previously stated. The properties of the outer layer of carbon and epoxy resin (a closely held trade secret) were estimated from physical measurements along with and a static spine test. A density of ρ=1590kg/m^3 was used, with orthotropic elastic properties. The fibre direction is along the arrow shaft with a Young's modulus of E_1=222GPa. Orthogonal to the fibre direction the Young's modulus E_2=E_3=9.2GPa was used. The shear moduli where estimated to be G_{12}=G_{13}=6.1GPa, and Poisson's ratios of v_{12}=v_{13}=0.2 and v_{23}=0.4 were used. These properties make up the required five independent constants to define the orthotropic elastic material. Finally the shear modulus G_{23} = 3.28GPa was calculated from formula $E_2/(2(1+v_{23}))$. It is noted that errors in these estimated material properties are expected to cause some errors in the results of the FE model.

The ProTour570 arrow had a length of 787.4mm giving a total of 9240 elements when the FE model was meshed. The ProTour380 had a length of 863.6mm giving a total of 9528 elements in the FE model. The ProTour570 had an outer diameter of 4.844mm and a maximum shell thickness of 0.822mm, while the ProTour380 had an outer diameter of 5.24mm and a maximum shell thickness of 1.02mm. The tapered section of the arrow was defined by dividing the shaft length into 50mm sections each of constant thickness. It is noted that these step discontinuities in the thickness may cause minor discrepancies in the results.

The FEA results for the natural frequencies are listed in Tables 3 and 4. Compared to the all aluminium arrow the composite arrows exhibit stiffer in-plane characteristics in the axial direction since the n=0, m=0 extension mode is not evident below 5kHz. Also, the composite arrow has many more breathing modes below 5kHz, indicating the lower modulus of elasticity in the material orthogonal to the carbon fibre direction.

This FE modelling provided insight into the vibrational behaviour of the different arrows and identified the pertinent

frequencies for conducting experimental measurements using the Polytec scanning laser vibrometer.

EXPERIMENTS

The experimental apparatus and procedures for testing composite archery arrows are detailed in the following sections. Design and development of test apparatus was required to enable the measurement of resonant frequencies and mode shapes of arrows with the scanning laser Doppler vibrometer (SLDV). The procedure for testing an archery arrow is detailed and the results of the experiments are presented.

Experimental apparatus

The experimental apparatus included a 1D laser vibrometer, a vibration actuator (mechanically or acoustically coupled), and a suitable frame to support the composite arrow specimen. The Polytec PSV-400 3D SLDV was used in the experiments in a 1D configuration. Only one laser head was used to measure the velocity of the vibrations in the specimen (see Figure 10). The velocity decoder (VD-07) provides a voltage proportional to the vibration in the direction of the laser to a maximum sensitivity of 1 (mm/s)/V.

Figure 10. Experimental apparatus

The vibration actuators used include a mechanical shaker, a compression driver and a speaker. The mechanical shaker was model LDS201/3 that has a velocity sine peak of 1.49 m/s with a moving mass of 0.020kg. The compression driver was a TU-50 unit from a TOA Electronic horn speaker power rated to 50W. The horn attachment was replaced by a cylinder with inner diameter of 25mm. The speaker used was a 80mm diameter diaphragm power rated to 3W. A speaker attachment was manufactured to direct the sound field into the long thin arrow specimens (see Figure 11). The support frame design included a base optical breadboard along with adjustable components to provide mounting points. The specimen can be positioned horizontally in the test rig by thin elastic threads. Adjustable mounting supports for the arrow specimen and the mechanical shaker were designed and manufactured fit for the purpose of experiments.
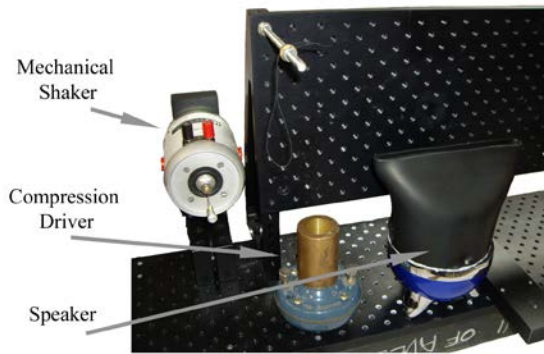
Figure 11. Experimental rig, with vibration actuators

The measurement of the vibrational behaviour of an object required an excitation source that vibrated the object which was measured by the laser scanning head. The Polytec PSV computer was used to generate the selected reference vibration excitation through a junction box. An amplifier with a gain of unity connected the reference signal to the selected vibration actuator. The mechanically or acoustically coupled vibration source was attached or positioned close to the object to be vibrated. Laser light from the scanning head is then directed at the object and a photo-detector within the scanning head will record the interference of the reflected light with a reference of the original laser light (Polytec, 2009). The controller decodes the signal to provide a voltage that is proportional to the velocity of the vibrating object. The voltage signal is digitised in the junction box and recorded by the computer. A video camera is positioned close to the scanning head to give live video feedback. Figure 12 shows a flow chart of control and measurement signals a diagram of the experimental apparatus.
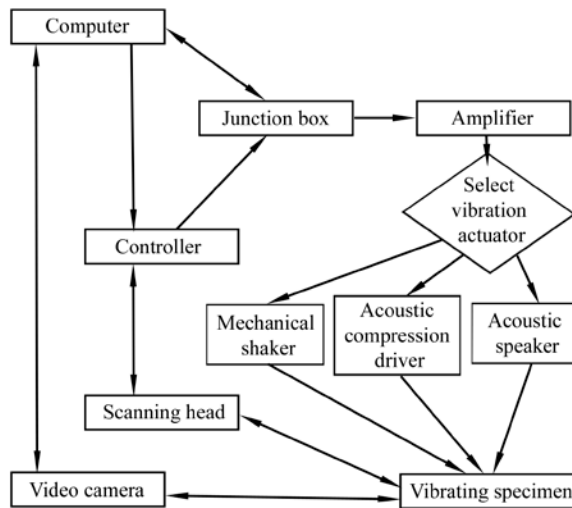
Figure 12. Experimental apparatus flow chart of control and measurement signals

The Polytec software presents the recorded information in either the time domain or frequency domain. The time domain signal of velocity is transformed to the frequency domain using a Fast Fourier Transform (FFT). The frequency response function and coherence can be monitored while the laser scanning process is taking place. After the scan is complete the software can process the data to display mode shapes for selected frequency bands. The measured data may also be exported and analysed in other software applications such as MATLAB.

Experimental procedure

The procedure for the experiments using the SLDV covers the set-up of the hardware and software. The following description provides a guide to the settings that were used for this research project.

Preparation of the arrow specimens required that the surface of the object have suitable reflective properties for reflecting the laser light. The surface of the specimen was sprayed with ARDROX 9D1B, a reflective and non-aqueous wet developer. The specimen was suspended horizontally in a suitable position in the test rig by thin elastic threads. The selected vibration actuator, either the mechanical shaker, acoustic compression driver or speaker was positioned at a non-symmetrical point along the length of the specimen.

The position of the laser scanning head was set perpendicular to and at the centre of the specimen to be scanned. For optimum vibrometer signals the recommended deflection angle of 10° was used for a specimen of 700mm length. The optimum distance for signal level is achieved when the object is in a maximum of the laser intensity. It was determined that the optimal standoff distance was 1935mm. The video camera was positioned close to the laser scanning head and adjusted to capture the area of object to be scanned.

The PSV 8.7 computer application settings control the input and output signals of the experiment. The input signals include a reference signal from the generated vibration signal and the signals from the scanning head. The output signal was generated for the selected waveform and frequency. The following data acquisition parameters were used:

- General: FFT measurement mode with complex averaging of 75 with the remeasure option on.
- Frequency: Bandwidth selected for these experiments have been 1kHz, 4kHz, or 8kHz. The FFT lines of 1600 where used for most experiments. Overlapping of 75% is used to reduce the measurement time.
- Window: The rectangle window function is used for pseudo random generated waveform. The pseudo random signal is periodic in the time window and therefore will generate no leakage effects in the spectrum calculated by the FFT.
- SE: Signal Enhancement is used for the vibrometer channel, with the speckle tracking turned to a standard level to enhance the signal.
- Vibrometer: The velocity is set to 10mm/s/V for the mechanical shaker, or 1mm/s/V for the acoustic actuators. The tracking filter is off and the low pass filter set to suit the bandwidth. No high pass filter is used.
- Generator: Select pseudo random waveform recommended for simulated stochastic excitation. The wait for steady state was not required for these experiments.

A full scan of each test specimen was performed that measured a predefined single line of points on the object. Forty scan points were used for a bandwidth of greater than 4kHz to capture the higher frequency shapes, while twenty scan points were sufficient for experiments in the lower frequencies when there were less than six bending waves along the length of the specimen. The time required for the scan depended on the data acquisition parameters selected (typical time was 15 minutes). The scan was monitored to ensure good coherence between the generated vibration signal and the measured velocity signal.

Experimental results

The experiments on the all aluminium Superlite1712 arrow shaft were conducted to test the experimental procedures. The results were compared to the analytical calculations and FE results. The results of the experimental tests are presented as in Table 4. The mode indicies of each resonance frequency was determined through observation of the operational deflection shapes. The first two bending modes measured while using the speaker actuator are shown in Figures 13 and 14.

Table 4. Comparison of FEA natural frequencies to measured resonance frequencies for the Superlite1713 (Hz). Results are an average of tests on two sample arrows.

FEA	Shaker	Driver	Speaker	Mode indices
84	57	82	81	$n=1, m=2$
230	190	227	226	$n=1, m=3$
451	394	442	444	$n=1, m=4$
743	678	732	729	$n=1, m=5$
1107	1032	1090	1090	$n=1, m=6$
1541	1451	1518	1519	$n=1, m=7$
2044	1933	2013	2014	$n=1, m=8$
2222	2226			$n=0, m=1$
2613	2512	2575	2570	$n=1, m=9$
3248	3089	3203	3203	$n=1, m=10$
3622	3460			$n=0, m=0$
3947	3883	3892		$n=1, m=11$
4443				$n=0, m=2$
4706	4603			$n=1, m=12$

The results with the mechanical shaker did not correlate well with the resonant frequencies predicted by the FEA for the first six modes of vibration. It was determined that the physical connection of the mechanical shaker reduced resonance frequencies significantly and altered the mode shapes from the desired free-free boundary conditions. The moving mass of the shaker and the stinger attachment connection to the specimen increased the mass of the vibrating structure to cause these errors.
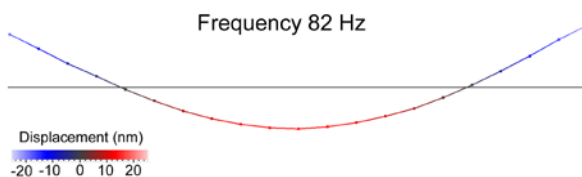
Figure 13. Experimental first bending mode of aluminium cylinder, modal indices $n=1, m=2$
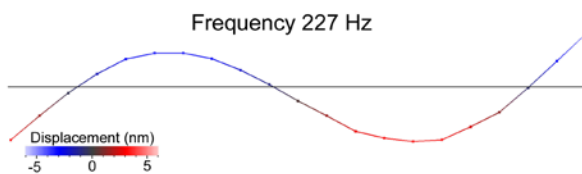
Figure 14. Experimental second bending mode of aluminium cylinder, modal indices $n=1, m=3$

For the first six modes of vibration, experiments using both acoustic vibration actuators showed good correlation to analytical and FE modelling. Neither of the acoustic vibration actuators coupled well with the specimens, although they showed a coherence of close to unity at the resonant frequencies. The mechanical shaker had excellent coherence, with the best correlation to the FE models for modes at high frequencies above 4kHz. The compression driver vibration method produced the best coherence and correlation in the range of 1kHz to 4kHz. The speaker vibration actuator pro-

duced the best coherence and correlation at the low frequency range below 1kHz. The following coherence graphs show the mechanical shaker (see Figure 15), the compression driver (see Figure 16), and the speaker actuator (see Figure 17).
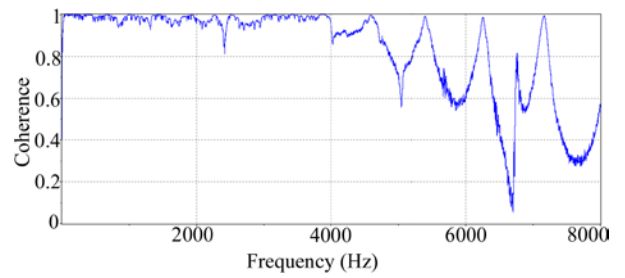
Figure 15. Coherence for mechanical shaker for 8kHz
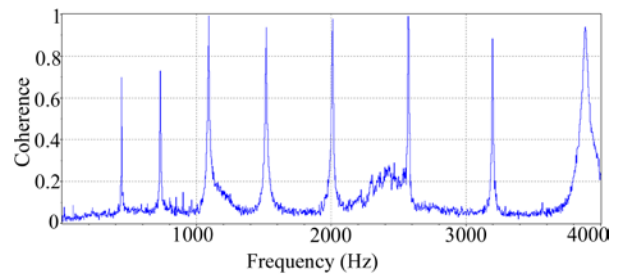
Figure 16. Coherence for compression driver for 4kHz
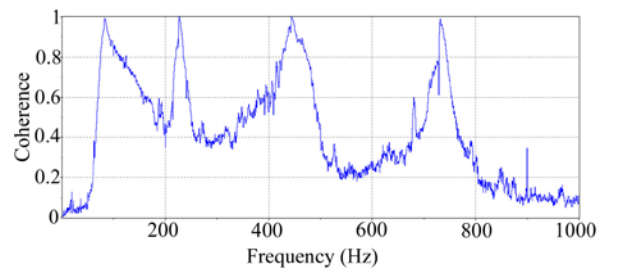
Figure 17. Coherence for speaker actuator for 1kHz

The experiments on the composite arrows where conducted using the mechanical shaker for the higher frequencies, and the compression driver and speaker for the lower frequencies. The results of the experimental tests are presented in Table 5. Each actuator was used in two tests on every arrow specimen, making a total of six experiments for each ProTour570 arrow tested.

Table 5. Comparison of FEA natural frequencies to measured resonance frequencies for the ProTour570 (Hz). Results are presented as mean±standard deviation.

FEA	Shaker	Driver	Speaker	Mode indices
91.9	63±2	91±0	91±1	$n=1, m=2$
250	206±2	247±2	247±1	$n=1, m=3$
486	423±5	480±3	479±3	$n=1, m=4$
794	714±9	788±3	787±5	$n=1, m=5$
1173	1082±15	1169±8	1172±8	$n=1, m=6$
1201				$n=0, m=1$
1617	1520±20	1624±8	1624±10	$n=1, m=7$
2122	2084±23	2145±12	2146±13	$n=1, m=8$
2390				$n=0, m=2$
2684	2620±28	2735±9	2729±17	$n=1, m=9$
3300	3219±32	3382±10		$n=1, m=10$
3578				$n=0, m=3$
3964	3784±44			$n=1, m=11$
4672	4748±51			$n=1, m=12$

The same experiments were conducted on the ProTour380 arrows. The results of the experimental tests are presented in Table 6.

Table 6. Comparison of FEA natural frequencies to measured resonance frequencies for the ProTour380 (Hz). Results are presented as mean±standard deviation

FEA	Shaker	Driver	Speaker	Mode indices
83.0	59±1	84±1	83±2	$n=1, m=2$
221	181±3	218±1	217±1	$n=1, m=3$
426	372±2	422±2	422±1	$n=1, m=4$
697	633±2	698±2	697±3	$n=1, m=5$
1032	958±4	1034±5	1034±1	$n=1, m=6$
1147				$n=0, m=1$
1429	1345±6	1436±3	1434±4	$n=1, m=7$
1883	1775±13	1896±4	1897±8	$n=1, m=8$
2201				$n=0, m=2$
2385	2346±10	2415±3	2413±5	$n=1, m=9$
2932	2878±4	2991±8		$n=1, m=10$
3343				$n=0, m=3$
3523	3425±17	3612±7		$n=1, m=11$
4160	3757±64			$n=1, m=12$

In compiling the results for the mechanical shaker it was difficult to determine which resonance frequencies were bending modes and which were breathing modes of vibration. This difficulty is due to the fact that the bending modes of vibration have a greater deflection and velocity than the breathing modes. Using the 1D configuration on the SLDV also limited the identification of these modes, which could be improved by using the 3D configuration for experiments. There is less confidence in the accuracy of the resonant frequencies found with the mechanical shaker than those found with both the acoustic actuators.

The first resonance frequency from both composite arrows was used to calculate the damping ratio and to determine the difference between the calculated natural frequency and the measured resonance frequency. This used Equations (6) and (7) (Inman, 2001).

$$\zeta = \Delta f \, / \, (2\,f) \qquad (6)$$

$$\omega_r = \omega_n \, \sqrt{(1 - 2\,\zeta^2\,)} \qquad (7)$$

where ζ is the damping ratio, Δf is the modal bandwidth of the frequency response function at a point 3dB down from the peak, f is the mode centre frequency, ω_r is the resonance frequency, and ω_n is the natural frequency.

The damping ratio for the composite arrows was less than 0.01. Thus, for these composite archery arrows the measured resonance frequency is approximately equal to the natural frequency.

Comparing the results of both acoustic actuators to the FEA results for both the ProTour570 and ProTour380 as listed in Tables 3 and 4 respectively, the bending modes have an error of < 3%. Although the limitations in the material properties of the FE model are noted, the results show good correlation with the experimental results from both acoustic vibration actuators.

CONCLUSION

This paper has documented the preliminary work into modelling a composite archery arrow. As seen in the analytical and FE simulations, bending dominates the first modes of vibra-

tion. Experimental measurements have shown good correlation to the FEA results. The experiments conducted to date indicate the viability of the experimental procedures for future testing of composite archery arrows. The data gathered will provide a good base for comparison to damaged composite arrows.

While using composite materials offers the advantage of high strength and stiffness combined with low weight, the disadvantage of using this material is that damage may occur by fatigue and impact loads. Future work will be conducted to identify the vibrational behaviour of damaged composite arrows. Vibration prediction and modelling is important for monitoring the structural health of composite materials and understanding their performance in-service. The ideal outcome of future studies is to recommend a structural health monitoring procedure that could predict the decrease in performance of a composite arrow by measuring the vibrational behaviour.

ACKNOWLEDGEMENTS

REFERENCES

Easton 2011, *Easton Target 2011*, Easton Technical Products, viewed 12 May 2011, <http://www.eastonarchery.com/pdf/easton-2011-target-catalog.pdf>.

Egle, DM & Sewall, JL 1968, An analysis of free vibration of orthogonally stiffened cylindrical shells with stiffeners treated as discrete elements, *AIAA Journal*, vol. 6, no. 3, pp. 518-526.

Fahy, F & Gardonio, P 2007, *Sound and structural vibration: radiation, transmission and response*, 2nd edn, Elsevier, Oxford.

Forsberg, K 1966, Axisymmetric and beam-type vibrations of thin cylindrical shells, *4th Aerospace Sciences Meeting*, American Inst. Of Aeronautics and Astronautics, paper. 66-447

Gere, JM 2001, *Mechanics of Materials*, 5th edn, Nelson Thornes, London.

Hamidzadeh, HR & Jazar, RN 2010, *Vibrations of Thick Cylindrical Structures*, Springer, New York.

Inman, D 2001, *Engineering Vibration*, 2nd edn, Prentice-Hall, New Jersey.

Klopsteg, P 1943, Physics of bows and arrows, *American Journal of Physics*, vol. 11, pp. 175-192.

Kornecki, A 1971, Note on beam type vibrations of circular cylindrical shells, *Journal of Sound and Vibration*, vol. 14, no. 1, pp. 1-6.

Leissa, AW 1993, *Vibrations of Shells*, Acoustical Society of America through the American Institute of Physics, New York.

Park, JL 2011, The behaviour of an arrow shot from a compound archery bow, *Proceedings of the Institution of Mechanical Engineers, Part P: Journal of Sports Engineering and Technology*, vol. 225, no. P1, pp. 8-21.

Polytec 2009, *Theory Manual Polytec Scanning Vibrometer PSV-3D As Of Software 8.5*, Polytec, <http://www.polytec.com>

Zanevskyy, I 2001, Lateral deflection of archery arrows, *Sports Engineering*, vol. 4, no. 1, pp. 23-42.